Biochimica et Biophysica Acta 1837 (2014) 1271–1283

Contents lists available at ScienceDirect

Biochimica et Biophysica Acta

journal homepage: www.elsevier.com/locate/bbabio

Regulation of brain-type creatine kinase by AMP-activated protein kinase: Interaction, phosphorylation and ER localization

Sacnicte Ramírez Ríos [a,b,1], Frédéric Lamarche [a,b], Cécile Cottet-Rousselle [a,b], Anna Klaus [a,b], Roland Tuerk [c], Ramon Thali [c], Yolanda Auchli [d], René Brunisholz [d], Dietbert Neumann [c,2], Luc Barret [a,b], Malgorzata Tokarska-Schlattner [a,b], Uwe Schlattner [a,b,*]

[a] Univ. Grenoble Alpes, Laboratory of Fundamental and Applied Bioenergetics, Grenoble, France
[b] Inserm, U1055, Grenoble, France
[c] Institute of Cell Biology, ETH Zurich, Switzerland
[d] Functional Genomics Center Zurich, ETH Zurich/University of Zurich, Switzerland

ARTICLE INFO

Article history:
Received 10 February 2014
Received in revised form 25 March 2014
Accepted 31 March 2014
Available online 12 April 2014

Keywords:
Protein kinase
Creatine kinase
Endoplasmic reticulum
Energy homeostasis
Protein phosphorylation
Subcellular localization

ABSTRACT

AMP-activated protein kinase (AMPK) and cytosolic brain-type creatine kinase (BCK) cooperate under energy stress to compensate for loss of adenosine triphosphate (ATP) by either stimulating ATP-generating and inhibiting ATP-consuming pathways, or by direct ATP regeneration from phosphocreatine, respectively. Here we report on AMPK-dependent phosphorylation of BCK from different species identified by *in vitro* screening for AMPK substrates in mouse brain. Mass spectrometry, protein sequencing, and site-directed mutagenesis identified Ser6 as a relevant residue with one site phosphorylated per BCK dimer. Yeast two-hybrid analysis revealed interaction of active AMPK specifically with non-phosphorylated BCK. Pharmacological activation of AMPK mimicking energy stress led to BCK phosphorylation in astrocytes and fibroblasts, as evidenced with a highly specific phospho-Ser6 antibody. BCK phosphorylation at Ser6 did not affect its enzymatic activity, but led to the appearance of the phosphorylated enzyme at the endoplasmic reticulum (ER), close to the ER calcium pump, a location known for muscle-type cytosolic creatine kinase (CK) to support Ca^{2+}-pumping.

1. Introduction

A key element in sensing energy stress at the cellular and whole-body level is AMP-activated protein kinase (AMPK). This evolutionary conserved, heterotrimeric serine/threonine kinase integrates various inputs on the energy and nutritional state to finally trigger a large variety of cellular responses to relieve energy stress (reviewed in [1–4]). AMPK is activated covalently by phosphorylation of its α-subunit at Thr172 under the control of different upstream kinases and phosphatases that convey regulation by *e.g.* Ca^{2+} and various hormones. During energy stress, AMPK is activated by increased levels of AMP and also ADP [4–7] binding to the γ-subunit. They act *via* direct allosteric activation, promotion of phosphorylation at Thr172 and inhibition of dephosphorylation by phosphatases, involving a conformational switch as shown by us and others [8–10].

Activated AMPK directly acts on enzymes to regulate metabolic pathways or other signaling cascades, or to activate transcription factors for long term adaptation of energy metabolism. AMPK has further functions beyond energy homeostasis, *e.g.* in controlling cell cycle, shape, motility and proliferation (reviewed in [2,3]). Its involvement in metabolic and proliferation signaling proposed the kinase as a pharmacological target for type II diabetes and cancer (reviewed in [11–14]).

Isoforms of creatine kinase (CK) are essential parts of an intricate cellular energy buffer and transport system based on creatine (Cr) and phosphocreatine (PCr) that has been described in much detail by us and others [15–19]. Cellular uptake of Cr is controlled by a specific transporter [20]. CK then catalyzes the reversible transfer of high-energy phosphates between ATP and Cr to yield ADP and the high energy intermediate phosphocreatine (PCr). In cells with elevated and variable energy demands, in particular in muscle and brain, the CK

Abbreviations: ACC, acetyl-CoA carboxylase; AICAR, aminoimidazole carboxamide ribonucleotide; AMPK, AMP-activated protein kinase; BCK/MCK/uMtCK/sMtCK, isoforms of creatine kinase brain-type cytosolic/muscle-type cytosolic/ubiquitous and sarcomeric mitochondrial; CamKKβ, calmodulin kinase kinase beta; CPAE, cellulose polyacetate electrophoresis; Cr, creatine; PCr, phosphocreatine; ER, endoplasmic reticulum; hBCK, human BCK; MS, mass spectrometry; PDI, protein disulfide-isomerase; PKC, protein kinase C; SERCA, sarcomeric/endoplasmic reticulum Ca^{2+}-ATPase; WT, wild-type

* Corresponding author at: Inserm U1055 and Univ. Grenoble Alpes, LBFA, BP 53, F-38041 Grenoble Cedex 9, France. Tel.: +33 476 51 46 71; fax: +33 476 51 42 18.
E-mail address: uwe.schlattner@ujf-grenoble.fr (U. Schlattner).
[1] Current address: Grenoble Inst. of Neurosciences, Inserm U836, Univ. Grenoble Alpes, Grenoble, France.
[2] Current address: Dept. of Molecular Genetics, Maastricht University, Maastricht, The Netherlands.

http://dx.doi.org/10.1016/j.bbabio.2014.03.020
0005-2728/

system maintains stable ATP/ADP ratios and thus regulates energy homeostasis [15,17,19]. CK isoforms accumulate PCr within the cell to high concentrations (up to 15 mM in brain) and use this otherwise inert compound in the reverse reaction to regenerate global and local ATP pools under conditions of increased workload (energy buffer function). They also exploit the rapid diffusibility of PCr to connect cellular sites of ATP generation (*e.g.* mitochondria) with sites of high ATP consumption (*e.g.* myofibrils or ion pumps; energy shuttle function). To fulfill these specific cellular functions, CK isoforms do not behave as strictly soluble enzymes, but partially associate with defined cellular structures. Based on the X-ray structures of banana-shaped cytosolic CK dimers and cuboidal octameric mitochondrial CK isoenzymes (MtCK) solved by us and others [21–24], the functioning of this membrane bound CK has been elucidated in molecular detail. MtCK co-localizes with mitochondrial adenylate translocase in proteolipid complexes to access matrix ATP for efficient PCr generation [15,25,26]. Cytosolic muscle-type CK (MCK) interacts with proteins in the myofibrillar M-line (myomesin, M-protein) and co-localizes with the sarcoplasmic/endoplasmic reticulum calcium pump (Ca^{2+}-ATPase, SERCA) to sustain massive, local regeneration of ATP from PCr for muscle contraction and Ca^{2+}-pumping, respectively [27,28]. In these cases, microcompartments are formed that allow direct channeling of ATP from CK to associated ATPases [28,29].

Much less is known in this respect for the cytosolic brain-type CK (BCK) found in the brain and most other non-muscle tissues. There is evidence from knockout mice and subcellular localization studies that the energy buffer and transport functions of the CK system are required to support high ATP turnover and correct functioning of brain cells. Knockout mice lacking BCK and brain MtCK (uMtCK) show a marked cognitive phenotype with deficiencies in learning and memory [30], spatial orientation [31], and in the functioning of hair bundle cells in the auditory system [32]. In the latter case, BCK allows for the very high ATP turnover (1 mM/s) imposed by the plasma membrane Ca^{2+}-ATPase pump to maintain Ca^{2+}-cycling. Like in the case of MCK, specific subcellular localization of BCK may be necessary for optimal local ATP supply. This notion is supported by co-localization of BCK with actomyosin in cortical microdomains of astrocytes and fibroblasts that affects cell shape and motility [33], or with F-actin in macrophages at the nascent phagosome that contributes to early steps in phagocytosis [34]. However, it is unknown how BCK is recruited to such specific cellular sites. That this may happen *via* direct protein/protein interactions is suggested by a study on thrombin signaling. Here, BCK directly interacts with the protein G-coupled thrombin receptor PAR-1 to provide ATP for efficient thrombin signaling and the associated cytoskeletal reorganization [35]. Whether such interactions are regulated remains an open question. Although BCK phosphorylation events can be found in earlier literature [36–38], they lack essential data like their effect on enzyme function and phosphorylation levels.

Functionally, the AMPK and CK systems cooperate in maintaining energy homeostasis within a cell [39]. While the CK system can react very rapidly to an acute energy challenge, AMPK is more involved in medium and long-term adaptations. A cross-talk between both systems has been postulated, including MCK interaction with and phosphorylation by AMPK [40]. However, both, the reported inhibition of MCK enzyme activity and, *vice versa*, AMPK-regulation by PCr/Cr ratios [40] could not be confirmed by follow-up studies [41–43]. Here we report on a specific phosphorylation of the BCK isoform at Ser6 by different AMPK isoforms that involves only transient interaction with AMPK. This phosphorylation does not affect enzymatic catalysis, but leads to the appearance of phospho-BCK at the endoplasmic reticulum (ER) and co-localization with the highly energy-demanding ER Ca^{2+}-pump. This is the first example that AMPK-mediated phosphorylation is not activating or inactivating an enzyme, but rather promoting a specific subcellular function.

2. Material and methods

2.1. Proteins

Rabbit BCK purified from brain was purchased from Sigma (St. Louis, USA). Chicken BCK (b subtype, B_b-CK, GeneID: 396248) subcloned into pET-3b (Novagen, Madison, USA), human BCK (GeneID: 1152) subcloned into streptavidin-fusion vector derived from pET-52b(+) (Novagen) and human BCK non-tagged subcloned into pET-42(+) vector (Novagen) were expressed in bacteria and purified by two-step chromatography as described earlier [21]. Site-directed mutagenesis of hBCK was performed by PCR using Phusion DNA polymerase (Finnzymes, Vantaa, Finland) and mutagenic primers. PCR products were purified with Nucleo Spin Extract II (Macherey Nagel) and self-ligated using T4 DNA ligase (New England Biolabs, Evry, France). All constructs were verified by DNA sequencing. Wild-type (WT) AMPK α1β1γ1 (111WT) and α2β2γ1 (221WT) isoform combinations, as well as the corresponding constitutively active forms mutated at αT172, α1T172Dβ1γ1 (111TD) or α2T172Dβ2γ1 (221TD) were expressed in bacteria from polycistronic vectors and purified by multi-dimensional HPLC as described earlier [8,44]. GST-CamKKβ fusion from pGEX-PreS-CamKKβ (kindly provided by H. Tokumitsu, Kagawa Medical University, Japan) and GST-ACC catalytic domain fusion construct (kindly provided by G. Hardie, Univ. of Dundee, UK) were expressed and purified as described earlier with some modifications [45].

2.2. Screening for AMPK substrates, mass spectrometry, Edman sequencing

Screening was performed according to the 'MudSeeK' protocol (38) with a modified protein pre-fractionation. Briefly, mouse brain lysates (180 mg protein, dialyzed against 10 mM HEPES, pH 8.5, 5% glycerol) were separated on an anion exchange column (Poros HQ, 4.67 ml bed volume, Life Technologies, Carlsbad, USA) with a linear salt gradient (0–1 M NaCl, 10 mM HEPES, pH 8.5). Protein in selected fractions was precipitated by stepwise addition of saturated ammonium sulfate solution (10% steps to 70% (v/v)). Each pellet was resuspended in 250–400 μl 20 mM HEPES pH 8 by vortexing and sonication for 5 min and salt removed by overnight dialysis against 20 mM HEPES pH 8. Resulting fractions were subjected to 1D- and 2D-screening as described [46]. Untagged hBCK was phosphorylated *in vitro* by constitutively active α1T172Dβ1γ1 AMPK (111TD), separated by SDS-PAGE, stained with colloidal Coomassie Blue, and radioactive gel bands excised. Tryptic digestion, peptide extraction, purification by reverse-phase chromatography and mass spectrometric analysis were performed as reported [47]. Selected radioactive peptides were sequenced by solid phase Edman degradation [48].

2.3. In vitro phosphorylation assays

In vitro phosphorylation of BCK was carried out as described [49,50]. Briefly, 240 pmol protein was incubated for 3 min at 37 °C in the presence or absence of 10 pmol AMPK 111TD in kinase buffer containing 200 μM [γ-^{32}P]ATP (with a specific activity of 400 mCi/mmol ATP), 50 μM AMP, 5 mM $MgCl_2$, 1 mM DTT, and 10 mM HEPES (pH 7.4). Alternatively, wild-type (WT) α1β1γ1 or α2β2γ1 AMPK (111WT, 221WT) was activated by 20 min incubation at 30 °C with 1 pmol CamKKβ in kinase buffer without radiolabel. BCK WT or mutants (200 pmol) were incubated for 3 min at 37 °C in the presence or absence of 3.5 pmol pre-activated 111WT or 221WT in kinase buffer. Kinase reactions were stopped by the addition of SDS sample buffer. Aliquots (9 μg protein) were subjected to 10% SDS-PAGE and autoradiography or analysis with a Typhoon phosphoimager (GE Healthcare, Vélizy, France).

2.4. Enzyme activity assays and gel filtration chromatography

Enzymatic activity of purified hBCK wild-type and mutants was measured with a photometer using a coupled enzyme assay as described for forward and reverse reactions [51]. Changes in the redox state of pyridine nucleotides were followed at 340 nm in a Specord 210 spectrophotometer (Analytikjena, Jena, Germany) thermostated at 25 °C. For the determination of dissociation rate constants (K_d, K_m), a matrix of initial velocity data was recorded by varying 5 different concentrations of each substrate at 5 different, fixed concentrations of the second substrate (0.5, 1, 2, 4 and 20 mM PCr; 0.02, 0.1, 0.2, 0.4 and 2.0 mM ADP; 0.5, 1, 2, 5 and 10 mM Cr; 0.1, 0.2, 0.8, 2 and 4 mM ATP). Mg salt concentrations were chosen to assure that ADP and ATP are entirely in their Mg^{2+}-complexed form. Data were analyzed by global fitting with a random equilibrium model (Sigma Plot Enzyme Kinetics Module). Gel filtration chromatography of pure BCK WT and mutant proteins was done with Superose 12 columns (GE Healthcare) and 25 mM Tris–HCl (pH 8.0), 150 mM NaCl and 2 mM β-mercaptoethanol at 1.0 ml/min and 10 °C. The column was calibrated for Stokes' radii with carbonic anhydrase (24.0 Å, 29 kDa), albumin (35.5 Å, 67 kDa), aldolase (48.1 Å, 158 kDa), catalase (52.2 Å, 232 kDa), ferritin (61 Å, 440 kDa) and thyroglobulin (70.0 Å, 669 kDa).

2.5. Yeast two-hybrid assays

Interaction of hBCK WT and S6D mutant with different AMPK subunits was analyzed by a cytosolic Y2H technique based on reconstitution of split-ubiquitin (cyto-Y2H, Dualsystems Biotech, Schlieren, Switzerland; [52]). Cloning procedures using Sfi1 sites, transformation of yeast cell line NMY51 and yeast spotting were performed as described [52]. The system was modified for anchoring interaction partners at the plasma membrane, not at the ER (unpublished data). Briefly, BCKs were expressed as plasma membrane-anchored fusion proteins (bait), while AMPK subunits were expressed as soluble fusion proteins (prey). Interactions activating reporter gene transcription allow growth on nutrient-deficient medium. Yeast cells were spotted on selective medium lacking tryptophan and leucine (SD-WL) as growth assay to verify the presence of bait and prey plasmid, and on medium lacking tryptophan, leucine, adenine and histidine (SD-AHWL) for protein interaction analysis. Spotted plates were incubated 72 h at 30 °C.

2.6. Cell culture and treatments

Primary astrocyte cultures were prepared aseptically from the cerebral hemispheres of three- to four-day-old mice pups as described previously [53] with some modifications. Pups were sacrificed by decapitation under sterile conditions. Cerebral hemispheres were dissected free of the meninx and gently dispersed in DMEM/F12 supplemented with 10% inactivated fetal calf serum and 1% penicillin, streptomycin and amphotericin B. The resulting cell suspension was centrifuged at 180 *g* for 5 min. The pellet was redispersed in the same serum-supplemented medium and filtered successively through cell strainers with 100 μm and 70 μm pores. The final concentration of the cell suspension was adjusted to 6×10^5 cells per milliliter of medium. The suspension was transferred into Petri dishes or glass coverslips coated with poly-L-lysine (10 μg/ml). Cells were maintained at a constant temperature of 37 °C in a humidified atmosphere containing 5% CO_2/95% air. Twenty-four hours after seeding, the culture medium was removed and replaced with fresh medium. Medium was changed every three days. Growth, density, and morphologic characteristics of the cells were observed regularly by phase-contrast microscopy. After 10 to 12 days in culture, the cells were shaken in order to eliminate microglia and oligodendrocytes. After 14 days *in vitro* (14 DIV), the monolayer typically consisted of more than 95% astrocytes, as demonstrated by positive immunostaining with the astrocyte marker glial fibrillary acidic protein (GFAP).

Mouse embryonic fibroblasts (MEFs), both WT and BAK −/− (BCK/AK1 double knockout MEFs) kindly provided by Bé Wieringa (University of Nijmegen, The Netherlands), were cultured as described [33]. When cultures were close to confluence (about 3 days of culture), they were treated for 30 or 60 min at 37 °C with 50 μM A-769662 (kindly provided by Grahame Hardie, Division of Molecular Physiology, College of Life Sciences, University of Dundee, UK) or 1 mM aminoimidazole carboxamide ribonucleotide (AICAR, Biotrend Chemicals, Zurich, Switzerland), dissolved in DMSO or water, respectively.

2.7. Immunoblotting, 2D-PAGE and cellulose polyacetate electrophoresis

Cortical astrocyte lysates were prepared as described [33] using lysis buffer containing protease inhibitor cocktail (Roche Diagnostics, Mannheim, Germany) and phosphatase inhibitor cocktail (GE Healthcare). Protein concentrations were determined with the Bradford-based Biorad microassay (Biorad, Reinach, Switzerland) and BSA as standard. Samples were resolved by 10% SDS-PAGE or 2D-PAGE and transferred to Hybond ECL nitrocellulose membrane (Amersham Biosciences, Buckinghamshire, UK). Membranes were washed 3× in Tris-buffered saline with 0.1% Tween-20 (TBST), incubated in TBST with 5% nonfat dry milk (TBST-M) for 1 h at room temperature (RT), washed again 3× in TBST, and incubated with the following primary antibodies diluted in TBST-M for 1 h at RT or overnight at 4 °C (if not stated otherwise, antibodies were from Cell Signaling Technology, Danvers, MA, USA): rabbit polyclonal antibodies against P-Thr172 AMP-activated protein kinase alpha (1:1000), P-Ser79 acetyl-CoA carboxylase (1:1000), total AMP-activated protein kinase alpha (1:1000), total BCK (1:2000; see [54]), and P-Ser6 BCK (1:1000). The anti-P-Ser6 BCK antibody was obtained by immunization of rabbits with the synthetic peptide PFSN(P~S)HNALKL (Eurogenetec, Angers, France), corresponding to the very N-terminal part of hBCK (amino acids 1–12), and affinity purification using the peptide employed for immunization. Membranes were washed 3× in TBST and then incubated in a TBST-M dilution of secondary antibodies coupled to horseradish peroxidase for 1 h at RT (1:5000). After 3× washing in TBST, immunoreactive bands were visualized by chemiluminescence (ECL plus, Amersham Biosciences, Buckinghamshire, UK) using film or quantified by an ImageQuant LAS4000 (GE Healthcare).

For 2D-PAGE, cortical astrocytes were lysed in 7 M urea, 2 M thiourea, 4% CHAPS, 40 mM DTT, 1.0% v/v IPG buffer, 0.5% v/v Triton X-100, protease inhibitor mix (Roche Diagnostics, Mannheim, Germany) and phosphatase inhibitor cocktail (GE Healthcare), sonicated, incubated for 1 h, centrifuged at 14,000 *g* for 60 min, and desalted with 2-D clean-up kit (GE Healthcare), all at 4 °C. Protein was determined with the 2D-Quant kit (GE Healthcare). About 500 μg protein was separated on an Ettan IPGphor 3 (GE Healthcare) with nonlinear gradient gel strips (pH 3–10, 24 cm; GE Healthcare) and 64,500 Vh (0 to 10,000 V during 12 h, constant voltage for 4 h). Strips equilibrated in 75 mM Tris–HCl pH 8.8, 6 M urea, 29.3% glycerol, 2% SDS, and 0.002% bromophenol blue (in the presence of 1% DTT (w/v) or 2.5% iodoacetamide (w/v), 15 min each) were applied to large 10% SDS-PAGE gels. After protein separation and fixation with 50% ethanol and 10% acetic acid for 1 h, gels were stained with colloidal Coomassie Blue (Roth, Karlsruhe, Germany) for 12 h and excess dye was washed out with distilled water.

For cellulose polyacetate electrophoresis (CPAE), astrocytes cultured for 14 days were incubated in the presence or absence of 50 μM A769662 for 30 min at 37 °C. Astrocyte lysates prepared as described [33] were separated by CPAE for 1 h at 150 V and at room temperature [55]. CPAE was performed on Cellogel strips (No. OlA42) in an electrophoresis tank (both from Biotec-Fischer, Reiskirchen, FRG) with running buffer (11.7 mM barbiturate, 52.4 mM diethylbarbiturate pH 8.6, 1.4 mM β-mercaptoethanol). CK bands were visualized by a color reaction coupled to CK enzyme activity in an agarose overlay gel [55,56].

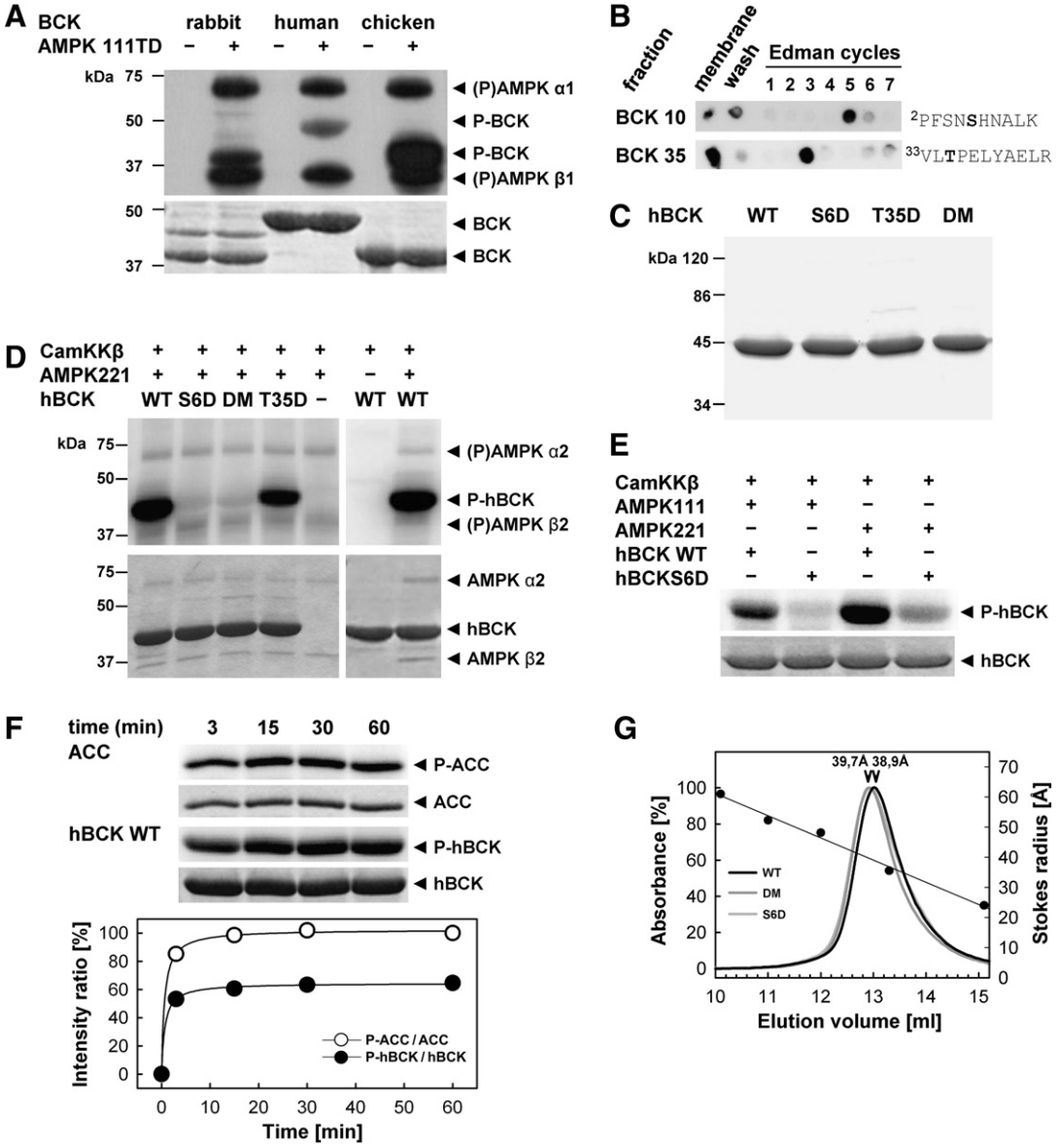

Fig. 1. BCK is phosphorylated by AMPK at serine 6. (A) Phosphorylation of BCK from different species. Autoradiograph (top) and Coomassie Blue stain (bottom, loading control) of SDS-PAGE showing *in vitro* phosphorylated rabbit, human (Strep-tagged), and chicken BCK (240 pmol each), incubated with [γ-32P]ATP in the presence (+) or absence (−) of constitutively active α1T172Dβ1γ1 AMPK (111TD, 10 pmol). (B) Identification of phospho-sites in human BCK (hBCK). Autoradiograph of solid phase Edman sequencing (seven cycles) identifying the position of [γ-32P]-labeled amino acids in the two tryptic phosphopeptides (see Suppl. Fig. S1) isolated from hBCK phosphorylated as in panel A; membrane, residual peptide after last Edman cycle; wash, unbound peptide. (C) Purity of WT and mutant hBCK shown by Coomassie Blue-stained SDS-PAGE (5 μg protein/lane). (D) Ser6 is the main hBCK site phosphorylated by AMPK. Autoradiograph (top) and Coomassie Blue stain (bottom, loading control) of SDS-PAGE showing *in vitro* phosphorylated WT and mutant hBCK (200 pmol each) performed as in panel A, but using AMPK α2β2γ1 WT (221WT, 3.5 pmol) activated by CamKKβ (1 pmol). Note: only S6D mutation precludes phosphorylation by AMPK. (E) hBCK is phosphorylated by AMPK111 and AMPK221. Autoradiograph and Coomassie Blue-stain of SDS-PAGE showing *in vitro* phosphorylated WT and S6D hBCK (200 pmol each) performed as in panel D. (F) hBCK and acetyl-CoA carboxylase (ACC) are phosphorylated at similar rates and stoichiometries. Autoradiograph and Coomassie Blue-stain of SDS-PAGE (top) showing *in vitro* phosphorylation time course of GST-ACC (80 pmol) and hBCK monomers (200 pmol) performed as in panel D. Quantification of incorporated radiolabel (bottom) is given as normalized to the protein amount (intensity ratio) of ACC (○) or BCK (●) monomers, relative to the maximal ACC signal. (G) Phospho-mimetic hBCK mutants display slightly increased Stokes radius. Separation of WT and mutant hBCK (0.3 mg each) on a calibrated Superose 12 column; elution volumes (Stokes radii) of BCK WT (black): 13.02 ml (38.9 Å); S6D (gray): 12.92 ml (39.7 Å); S6D–T35D (DM, dark gray); 12.94 ml (39.7 Å). Figures are representative of three repetitions. Abbr.: P-BCK, phospho-BCK; (P)AMPKα1, (P)AMPKβ1, autophosphorylated AMPK α1- and β1-subunits; hBCK, human BCK; WT, wild-type; DM, S6D/T35D double mutant.

2.8. Immunocytochemistry

Astrocytes grown on Lab-Tek chamber slides (Thermo Scientific Nunc, Rochester, NY, USA) were treated with AMPK activators as described above, rinsed twice with pre-warmed phosphate-buffered saline (PBS), and fixed with 3% paraformaldehyde in PBS. Following three washing steps in PBS, cells were permeabilized with 0.2% Triton X-100 in PBS. After extensive washing with PBS, cells were blocked for 1 h in PBS containing 3% bovine serum albumin (BSA) and 0.1% Tween 20, incubated 1 h at RT or overnight at 4 °C with primary antibodies diluted in blocking buffer, washed three times with blocking buffer and incubated with secondary antibodies in blocking buffer for 45 min at RT. Applied primary antibodies were rabbit anti-P-Ser6 BCK (1:100), mouse anti-PDI (1:100, ER marker, Abcam, Cambridge, UK) and chicken anti-BCK (1:200) [54]. Applied secondary antibodies were DyLight 649 (red fluorescence) conjugated either to goat–anti-rabbit (1:250, Jackson ImmunoResearch, Baltimore, USA), donkey–anti-mouse (1:250, Jackson ImmunoResearch), or donkey–anti-chicken

Table 1
Sequence alignment of BCK isoform species.

Sequence structure	hhhhhhhh hhhh		hhhhh hhhhh	
	1 10	20	30	40
Human BCK	MPFSN**S**HNALKLRFPAEDEFPDLSAHNNHMAKVL**T**PELYA			
Mouse BCK	MPFSN**S**HNTQKLRFPAEDEFPDLSSHNNHMAKVL**T**PELYA			
Rat BCK	MPFSN**S**HNTQKLRFPAEDEFPDLSSHNNHMAKVL**T**PELYA			
Rabbit BCK	MPFSN**T**HNTLKLRFPAEDEFPDLSAHNNHMAKVL**T**PEMDA			
Chicken BCK	MPFSN**S**HNLLKMKYSVDDEYPDLSVHNNHMAKVL**T**LDLYK			

Sequences are given for cytosolic BCKs from human (**P12277**, KCRB_HUMAN), mouse (**Q04447**, KCRB_MOUSE), rat (**P07335**, KCRB_RAT), rabbit (**P00567**, KCRB_RABIT) and chicken (**P05122**, KCRB_CHICK). Sequences of the proteins (with starting methionines and targeting peptides) are given. The conserved secondary structure is indicated on top (h, α-helix), residues homologous to Ser6 and Thr35 are indicated in bold letters.

(1:250, Jackson ImmunoResearch), as well as DyLight 488 (green fluorescence) conjugated goat–anti-rabbit (1:250, Jackson ImmunoResearch). Different cellular structures (plasma membrane, Golgi) were stained with 50 μg/μl of WGA (wheat germ agglutinin) directly coupled to Alexa Fluor 350 (Invitrogen). Nuclei were stained with 1 μM Hoechst dye (Interchim, Montlucon, France) and mitochondria with 250 nM Mitotracker Red CMXRos (Invitrogen) before permeabilization and immunostaining. Images were collected with a Leica TCS SP2 Acoustico Optical Beam Splitter (AOBS) inverted laser scanning confocal microscope equipped with a coherent 351–364 nm UV laser using a 63× water immersion objective (HCX PL APO 63.0 × 1.20 water corrected). Laser excitation was 351/364 nm for Hoechst (nuclei) and WGA, 488 nm for DyLight 488, 633 nm for DyLight 649 and 543 nm for Mitotracker Red CMXRos and PLA probes. Confocal pinhole (Airy units) was 1. Fluorescence emission bands were precisely adjusted using an AOBS at 415–480 nm for Hoechst, 505–540 nm for Dylight 488, 645–705 nm for Dylight 649, 580–660 nm for Mitotracker Red, and 575–655 nm for PLA-probes. In double staining of phospho-BCK and PDI, confocal sections of 0.5 μm z-step of both fluorescent signals were acquired sequentially and then merged. 3D reconstruction images were obtained using Volocity software (Improvision, France). Each experiment was performed on a randomly chosen field containing several cells.

2.9. Confocal 3D analysis and proximity ligation assay

A stack of nine confocal sections (z-series) was collected in 0.5 μm steps. Each plane of the z-stacks was subjected to Image J software for fluorescence intensity analysis and Volocity software for fluorescence correlation analysis. Correlation between two fluorescence channels is represented in a scatter diagram (cytofluorigram) of red voxels (y-axis) co-localized with green voxels (x-axis). The calculated co-localization coefficient for both channels yields values between zero (no co-localization) and one (complete co-localization) as described [57].

Co-localization analysis *in situ* based on proximity ligation was performed with the Duolink *In Situ* kit (Olink Bioscience, Uppsala, Sweden) according to the manufacturer's instructions. This assay detects also weak and transient interactions and co-localization with a maximum distance of ~30 nm. Primary antibodies used were rabbit polyclonal anti-P-BCK (diluted 1:100) and mouse monoclonal anti-SERCA2 (Pierce, diluted 1:500).

Table 2
Enzyme kinetic constants of human BCK wild-type and S6D mutant.

Kinetic parameter		hBCK proteins	
		WT	S6D
Forward reaction			
Specific activity	[U/mg protein]	29.0 ± 2.9	29.5 ± 2.8
K_d (MgATP)	[mM]	1.15 ± 0.05	1.11 ± 0.08
K_m (MgATP)	[mM]	0.88 ± 0.02	P0.86 ± 0.05
K_d (Cr)	[mM]	6.94 ± 0.26	7.05 ± 0.11
K_m (Cr)	[mM]	5.80 ± 0.16	6.07 ± 0.10
Reverse reaction			
Specific activity	[U/mg protein]	128.0 ± 3.5	127.0 ± 5.2
K_d (MgADP)	[mM]	0.19 ± 0.01	0.21 ± 0.02
K_m (MgADP)	[mM]	0.26 ± 0.01	0.29 ± 0.32
K_d (PCr)	[mM]	1.99 ± 0.12	2.02 ± 0.17
K_m (PCr)	[mM]	3.10 ± 0.17	3.00 ± 0.05

Constants for the hBCK wild-type (WT) and mutant (nS6D) forward and reverse reactions at pH 8 and 7, respectively, were calculated from initial rate data by global fitting using Sigma Plot software.

2.10. Cellular subfractionation

Embryonic mouse fibroblasts were lysed by extrusion *via* a 27 Ga needle and ER-enriched fractions were obtained by using the Endoplasmatic Reticulum isolation kit ER0100 (Sigma, St Louis, USA) according to the manufacturer's instructions, following the calcium precipitation method. Fractions were analyzed by immunoblotting using primary antibodies specific against sarcoplasmic/endoplasmic reticulum Ca^{2+}-ATPase 2 (SERCA2, mouse monoclonal, Pierce, diluted 1:2500), the α1-subunit of Na^+/K^+-ATPase (mouse monoclonal; Millipore, diluted 1:2500), total voltage-dependent anion channel (VDAC, rabbit polyclonal, a gift of M. Colombini, Univ. Maryland, USA; diluted 1:500) and chicken anti-BCK (1:200) [54]. For BCK detection, identical aliquots of the post-mitochondrial fractions were in addition calcium-precipitated to enrich for ER.

3. Results

3.1. BCK is phosphorylated by AMPK at Ser6

An *in vitro* screen to identify protein kinase targets, termed 'MudSeeK', has been applied to identify new candidate AMPK substrate proteins from mouse brain [46]. This approach combines multi-dimensional protein prepurification from brain extracts, *in vitro* phosphorylation assays, 2D-PAGE and mass spectrometry. By adding a modified pre-fractionation procedure involving ammonium sulfate precipitation, novel putative AMPK targets have been detected and one of them identified as BCK. *In vitro* phosphorylation assays with constitutive active α1T172Dβ1γ1

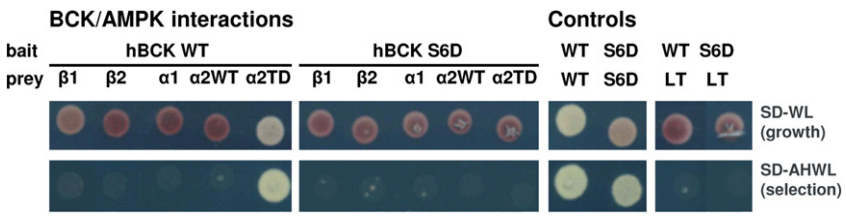

Fig. 2. BCK WT, not S6D mutant, interacts with active AMPK in yeast-two-hybrid assays. Interaction of wild-type (WT) or S6D hBCK with different AMPK subunits or αT172D (TD) mutant was analyzed by a cytosolic split-ubiquitin yeast two-hybrid assay. Controls show hBCK dimerization (positive control) and lack of interaction with an unrelated protein, *Simian virus* Large T antigen (negative control). Spots represent yeast grown for 72 h at 30 °C. Growth media: supplement-deficient (SD) in adenine (A), histidine (H), tryptophan (W) or leucine (L) allow verifying the incorporation of bait and prey plasmids (growth) and bait/prey interaction (selection).

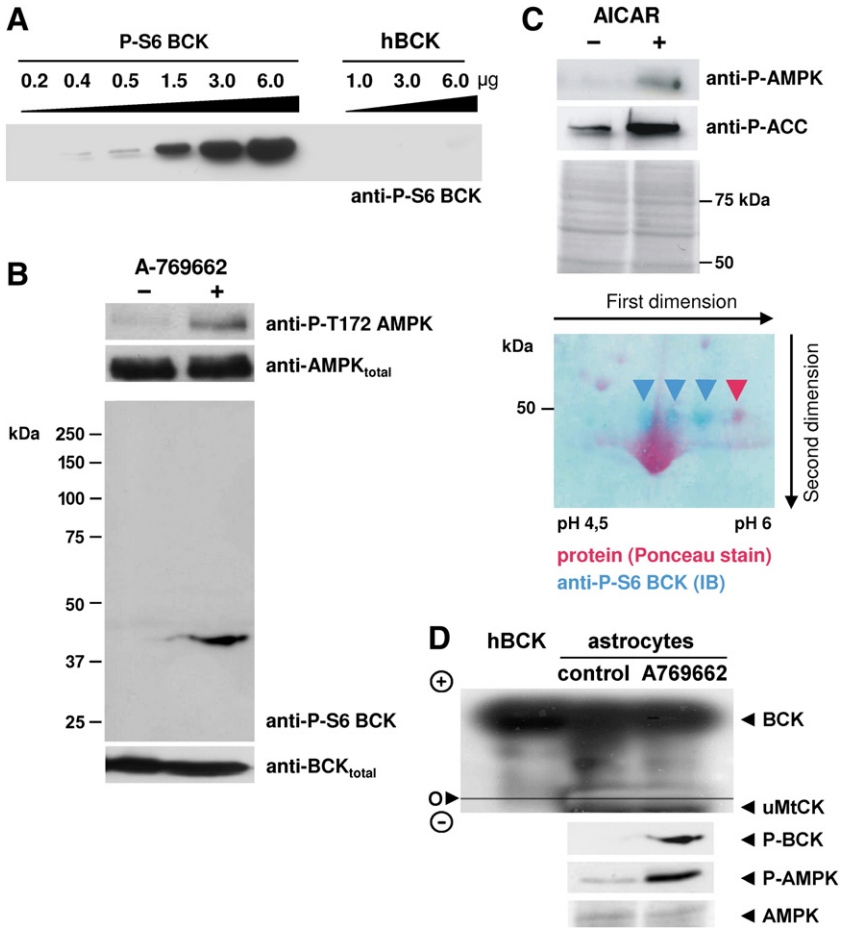

Fig. 3. P-Ser6 BCK is detected *in vitro* and in mouse astrocytes by a specific antibody. (A) Specificity and affinity of a purpose-made polyclonal antibody raised against P-Ser6 hBCK, tested by immunoblots of phosphorylated hBCK (0.2–6.0 µg) using constitutive active αT172Dβ2γ1 AMPK (221TD) or of non-phosphorylated controls. Note: No detection of even 6 µg non-phosphorylated hBCK. (B) Ser6-phosphorylation of murine BCK in primary mouse astrocytes, incubated for 30 min in DMED medium containing 50 µM A-769662 or vehicle only (DMSO). Representative SDS-PAGE-immunoblot of total cell lysates (60 µg protein/lane) probed for phosphorylated and total protein as indicated. (C) Ser6-phosphorylation of murine BCK in primary mouse astrocytes, incubated for 30 min in medium containing 1 mM AICAR or vehicle only (dH_2O). Upper panel: Representative SDS-PAGE-immunoblot of phosphorylated acetyl-CoA carboxylase (P-Ser79 ACC) and AMPK (P-Thr172) in total cell lysates (60 µg protein/lane); Ponceau stain shown as loading control. Lower panel: Overlay of protein (Ponceau-staining, red spots) and P-S6-BCK immunodetection (blue spots) in 2D-PAGE of total soluble protein (500 µg). (D) Enzyme activity of murine BCK is unaffected by Ser6-phosphorylation. Upper panel: Native cellulose polyacetate electrophoresis (CPAE) of hBCK (1 µg) and lysates of primary mouse astrocytes (40 µg) incubated for 30 min in DMED medium containing 50 µM A769662 or vehicle only (DMSO). CK bands were visualized by an enzyme-coupled assay that generates blue dye proportional to CK activity. Note: appreciation of BCK activity is achieved by separation of BCK from highly homologous mitochondrial CK. Lower panel: SDS-PAGE-immunoblots for P-Ser6 BCK and P-T172 AMPKα from these astrocyte lysates. Note: BCK activity is not affected by treatment with A769662; uMtCK bands migrate out of the gel. Figures are representative of three repetitions.

AMPK (111TD) and a 24-fold excess of pure rabbit, human and chicken BCK confirmed that vertebrate BCK is a very good *in vitro* substrate for AMPK (Fig. 1A).

To identify the involved residue(s), phosphorylated human BCK (hBCK) was subjected to tryptic digest and HPLC separation (Suppl. Fig. S1). The three radioactive fractions obtained (fractions 2, 10 and 35) were analyzed by MALDI-MS/MS, which revealed in two of them a phosphopeptide due to the typical loss of a phosphoric acid moiety (−98 Da; Suppl. Table 1 and Figs. S2, S3). Both peptides were in addition sequenced by Edman degradation, since there was some ambiguity with two serines being present in one of them (Fig. 1B). This combined approach identified two amino acids, Ser6 and Thr35, as putatively phosphorylated residues. Both are located in the N-terminal small domain of BCK; Ser/Thr residues at these positions are conserved across vertebrate species (Table 1).

To verify phosphorylation at Ser6 and Thr35, both residues were individually or together mutated into phospho-mimetic aspartic acid. The single mutants S6D and T35D and double mutant S6D/T35D (DM) were bacterially expressed, purified by two-step column chromatography to high purity (Fig. 1C), and subjected to *in vitro* phosphorylation assays with wild-type α2β2γ1 AMPK (221WT) pre-activated by the AMPK upstream kinase CamKKβ. While the T35D mutant still became strongly phosphorylated, S6D and S6D/T35D mutants incorporated only traces of radiolabel (Fig. 1D, left panels). Control experiments showed that these *in vitro* phosphorylations were only dependent on the presence of AMPK, not CamKKβ (Fig. 1D, right panels). Thus, Ser6 is the relevant AMPK phosphorylation site of hBCK.

Wild-type hBCK was phosphorylated by both AMPK complexes, 221WT and 111WT, when pre-activated with CamKKβ (Fig. 1G). The ratio of ^{32}P-incorporation into hBCK when incubated with the two activated AMPK complexes (221WT/111WT) was 2.5 for hBCK and 1.5 for acetyl-coA carboxylase (ACC), an AMPK reference substrate, suggesting hBCK to be a slightly better substrate for AMPK 221.

3.2. Ser6 is phosphorylated rapidly and at high levels comparable to ACC

The phosphorylation time course of hBCK WT and ACC, again using AMPK 221WT pre-activated by CamKKβ, revealed a similar and very rapid phosphorylation kinetics with half-maximal phosphorylation below 3 min and a maximum attained after 15 min (Fig. 1F). The total

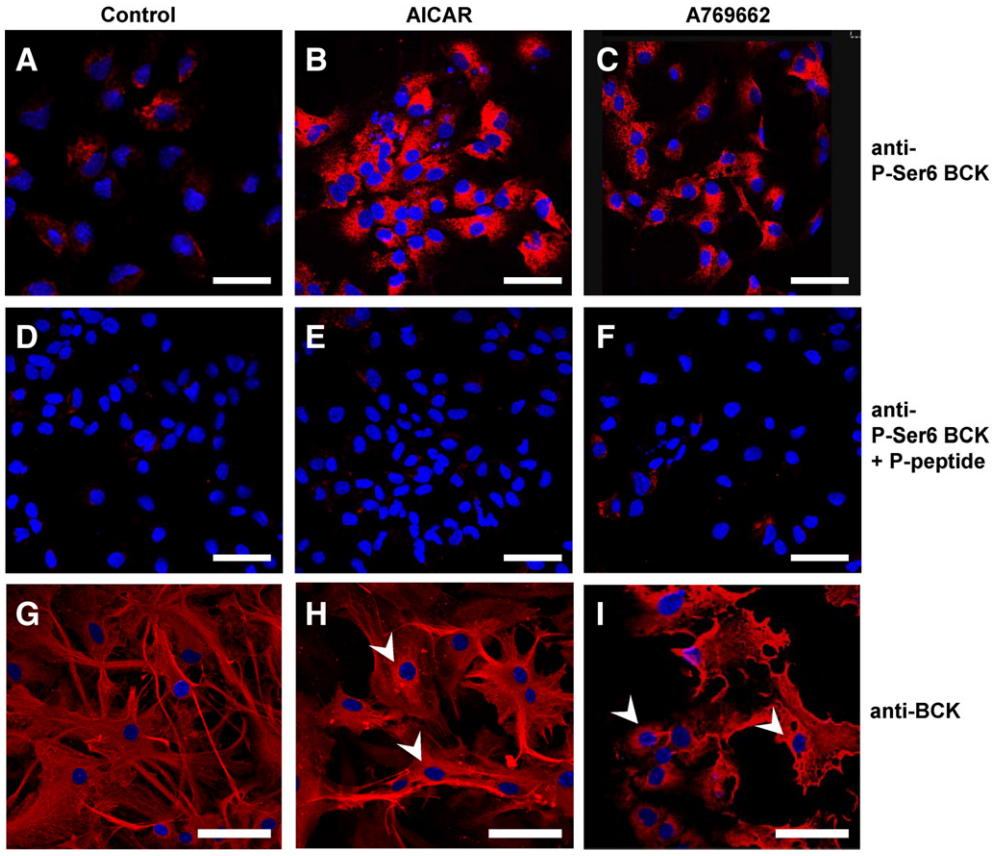

Fig. 4. Astrocyte P-Ser6 BCK localizes to perinuclear regions. Confocal microscopy images of primary mouse astrocytes fluorescently labeled for BCK (red) and nuclei (blue). (A–C) P-Ser6 BCK, (D–F) P-Ser6 BCK in the presence of P-peptide used for generating the anti-P-Ser6 BCK antibody (competition assay as specificity control), or (G–I) total BCK. Asytocytes were treated for 30 min (A,D,G) with vehicle only (dH_2O or DMSO) or with AMPK activators, either (B,E,H) 1 mM AICAR or (C,F) 50 μM A-769662. Scale bars: 47 μm (A–F) or 32 μm (G–I). Figures are representative of at least three repetitions. Arrows: increased peri-nuclear staining in panels H and I.

amount of radiolabel incorporated in hBCK is slightly more than half of what is found with ACC. The ACC construct that we have been using has only one AMPK phosphosite (Ser79) which can be almost stoichiometrically phosphorylated [58]. Since native BCK occurs as a dimer, the data suggest that one monomer per hBCK dimer is phosphorylated.

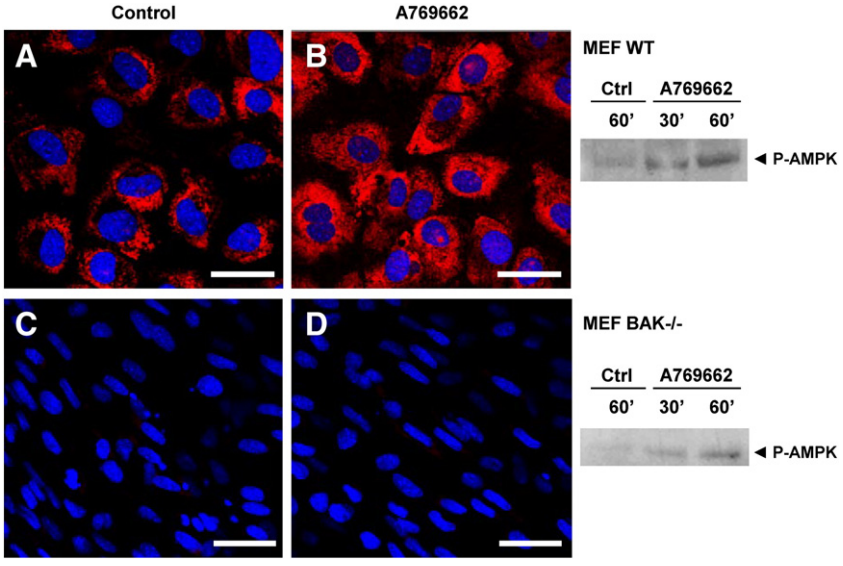

Fig. 5. P-Ser6 BCK is detectable upon AMPK activation in wild-type, but not BAK−/− fibroblasts. Confocal microscopy images of immortalized mouse embryonic fibroblasts (MEFs) from (A,B) control mice or (C,D) BAK−/− knockout mice, stained for P-Ser6 BCK (red) and nuclei (blue). MEFs were treated for 30 min (A,C) with vehicle only (DMSO) or (B,D) with AMPK activator A-769662 (50 μM). Scale bars: 35 μm (A–C) or 47 μm (D–F). Right panels: AMPK activation in control or BAK−/− MEFs treated in the same manner as above. MEF lysates were analyzed by SDS-PAGE immunoblotting (40 μg protein/lane) for P-αThr172 AMPK. Figures are representative of at least three repetitions.

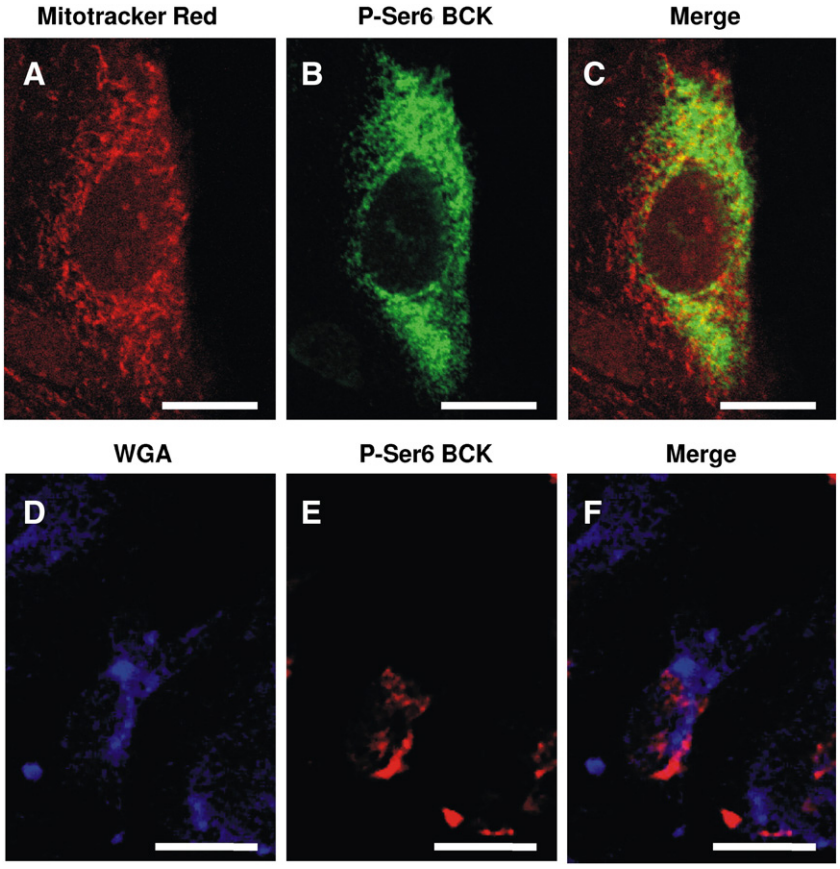

Fig. 6. Astrocyte P-Ser6 BCK does not co-localize with mitochondria or Golgi apparatus. Confocal microscopy images of primary mouse cortical astrocytes stained (A) with Mitotracker Red (mitochondrial marker, red fluorescence), (B) for P-Ser6 BCK (green fluorescence), (D) with wheat germ agglutinin (WGA, Golgi marker, blue fluorescence), or (E) for P-Ser6 BCK (red fluorescence); (C,F) merged images. AMPK was activated by 50 μM A-769662 (30 min, 37 °C). Scale bars: 26 μm.

3.3. Active AMPK interacts transiently with non-phosphorylated BCK via its α-subunit

To test how hBCK is recognized by AMPK, we applied a cytosolic yeast two-hybrid assay (cyto-Y2H). This *in vivo* interaction assay is very sensitive and can detect also weak or transient interactions. Its specificity was verified by the dimerization of the hBCK monomer (positive control) and hBCK interaction with *Simian virus* Large T antigen (negative control; Fig. 2). The assays clearly revealed interaction of hBCK WT with constitutively active AMPK α2T172D (α2TD), but not with inactive WT α1 or α2 subunits, while the S6D mutation prevented any formation of BCK/AMPK complexes (Fig. 2). The AMPK β subunits did not interact with hBCK neither. AMPK/BCK interactions were not detectable by co-immunoprecipitation (data not shown). Thus, AMPK substrate recognition is transient and requires activated AMPK α subunits and non-phosphorylated BCK.

3.4. S6D mutation or BCK phosphorylation do not alter enzymatic activity

We first examined whether BCK phosphorylation modifies its conformation or enzymatic activity. hBCK WT, S6D mutant and S6D/T35D double mutant were analyzed by calibrated gel filtration chromatography. This revealed only BCK species at a size of about 86 kDa, confirming that the dimeric quaternary structure of hBCK is preserved in phosphomimetic mutants (Fig. 1G). However, a small shift to larger Stokes radii in S6D mutant proteins indicated a slight conformational change. We further determined the precise kinetic parameters of recombinant hBCK WT and S6D mutant in both, forward and reverse directions of the two-substrate reaction (Table 2). The S6D mutation did not significantly alter enzyme kinetics in either direction of the reaction, and neither total specific activity, nor affinity values for the substrates, including K_m (binding as first substrate) and K_d (binding as second substrate). The same was observed with BCK that was phosphorylated *in vitro* by CamKKβ (data not shown) or with BCK isolated from mouse astrocyte cultures after pharmacological AMPK activation (Fig. 3D).

3.5. BCK is phosphorylated at Ser6 in astrocytes treated with A-769662 or AICAR

To further examine enzyme activity-independent functions of phosphorylated BCK, we developed a polyclonal rabbit antibody specific for the Ser6-phosphorylation of BCK (Fig. 3A). This antibody detected phosphorylated hBCK in immunoblots at high specificity, without cross-reactivity to non-phosphorylated BCK (up to 6 μg enzyme) or other proteins in immunoblots, and with a detection limit of about 400 ng hBCK.

BCK phosphorylation by AMPK *in vivo* was then examined in primary mouse cortical astrocytes. These cells have high and fluctuating energy demands and thus express elevated levels of BCK [33]. Astrocyte AMPK was activated with the pharmacological, cell-permeable activator A-769662 (Abbott Laboratories). Already 30 min treatment with 50 μM A-769662 led to strong AMPK activation *via* αThr172 phosphorylation in whole cell lysates (Fig. 3B). Using the anti-P-Ser6 BCK antibody, we detected a concomitant appearance of a single band of phospho-Ser6 murine BCK in whole cell extracts, which was absent in untreated controls. To confirm an AMPK-dependent phosphorylation of BCK in cells *in vivo*, we used AICA-riboside (AICAR) as a second pharmacological

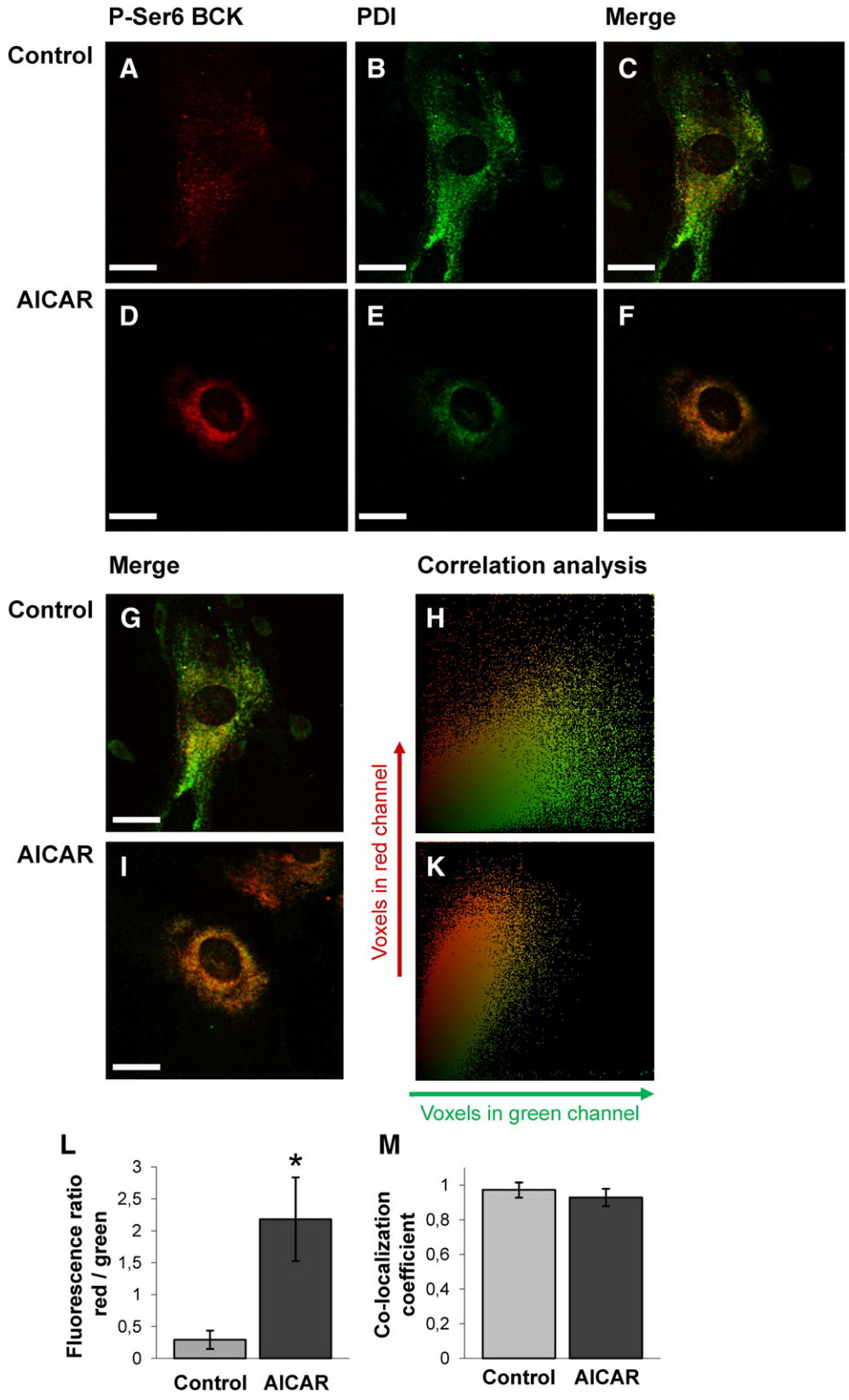

Fig. 7. Astrocyte P-Ser6 BCK fully co-localizes with endoplasmic reticulum in confocal 3D-analysis. 3D-reconstruction of primary mouse astrocytes, treated for 30 min with (A–C) vehicle only (dH_2O) or (D–F) 1 mM AICAR, and stained for (A,D) P-Ser6 BCK (red) or (B,E) ER marker protein disulfide isomerase (PDI, green); (C,F) merged signals. These images are representative of five randomly chosen fields, for each of which a stack of nine confocal sections was obtained (z-series) using 0.5 μm step width per plane (a gallery is shown in Suppl. Fig. S4). (G,I) Merged pictures of the entire z-stack. (H,K) Correlation analysis of all z-stacks for both fluorescence channels (scatter diagram; for details see Material and methods). (L) Fluorescence intensity ratio of the red channel to the green channel as a measure of P-Ser6 BCK signal increase relative to PDI. (M) Co-localization coefficient for the red and green channels as a measure of P-Ser6 BCK/PDI co-localization, determined from Fig. 6H,K; data given as mean ± SD (n = 5), *$p < 0.001$. Scale bar: 26 μm.

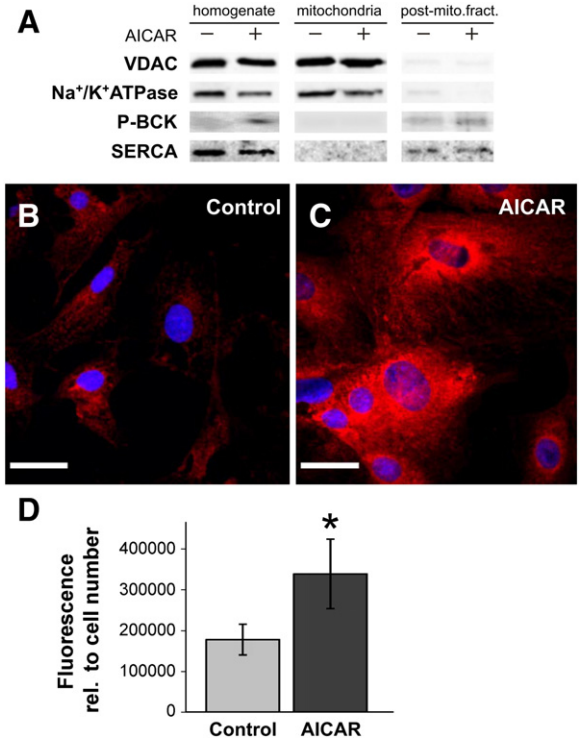

Fig. 8. Fibroblast P-Ser6 BCK co-purifies with ER and co-localizes with ER calcium pump. Immortalized mouse embryonic fibroblasts were treated for 30 min with vehicle only (dH_2O) or 1 mM AICAR. (A) Cellular subfractionation revealing increased co-purification of murine BCK with ER-enriched postmitochondrial fraction after AICAR-treatment. Crude homogenate, mitochondrial and post-mitochondrial fractions were subjected to SDS-PAGE-immunodetection for mitochondrial voltage-dependent anion channel (VDAC), plasma membrane Na^+/K^+-ATPase, P-Ser6 BCK (P-BCK), and sarcoplasmic/endoplasmic reticulum Ca^{2+}-ATPase 2 (SERCA). Representative blots of two independent experiments. For further details see Material and methods. (B–D) Proximity ligation assay revealing co-localization of P-Ser6 murine BCK with sarcoplasmic/ER Ca^{2+}-pump (SERCA). Mouse embryonic fibroblasts (MEFs) treated for 30 min with (B) vehicle only (dH_2O) or (C) 1 mM AICAR, labeled with anti-P-BCK and anti-SERCA2 antibodies, and further processed with the proximity ligation assay duolink kit (red fluorescence). Nuclei were stained with 1 μM Hoechst (blue fluorescence). Images are representative of three randomly chosen fields. Scale bar: 31 μm. (D) Ratio of red fluorescence normalized to cell number (number of nuclei), which corresponds to the amount of P-Ser6 BCK co-localizing with SERCA2. Images were analyzed with Image J and Volocity software; data are given as mean ± SD (n = 3), *p < 0.01.

activator with an entirely different action mechanism. Treatment of mouse primary astrocytes with 1 mM AICAR for 30 min also led to phosphorylation of AMPK (at αThr172) and its direct substrate ACC (at Ser79; Fig. 3C). 2D-PAGE protein separations revealed three equally spaced P-Ser6 BCK spots with the same Mr, not seen in controls. Thus, Ser6 phosphorylation of BCK occurs in astrocytes *in vivo* and is present in different murine BCK species, likely differing by additional (auto) phosphorylation events.

3.6. Ser6-phosphorylated BCK localizes to central, perinuclear cellular regions

In search of a function for AMPK-mediated phosphorylation of BCK, we investigated putative effects on murine BCK subcellular localization by immunocytochemistry and confocal microscopy in the astrocyte model (Fig. 4). Indeed, while untreated astrocytes presented only low levels of P-Ser6 BCK (Fig. 4A), AMPK activation by two different pharmacological activators (AICAR and A-769662) led to the appearance of P-Ser6 BCK in the cell center, including the perinuclear region (Fig. 4B, C). Bulk BCK in astrocytes is quite homogeneously distributed within the cytosol, with some enrichment close to the plasma membrane and in the many unbranched cellular processes (Fig. 4G). Activation of AMPK by AICAR or A-769662 changed this distribution only slightly by increasing the peripheral signals, but also inducing some faint perinuclear staining (Fig. 4H,I, see white arrows). This suggests that P-Ser6 BCK represents only a minor fraction of bulk cytosolic BCK.

To verify the specificity of anti-P-Ser6 antibody in these *in vivo* applications, two different control experiments were performed. First, we applied a competition assay with the P-peptide that had been used for the generation of the anti-P-Ser6 antibody. This led to an almost complete disappearance of the P-Ser6 BCK signal (Fig. 4D–F). Second, we used immortalized mouse embryonic fibroblasts (MEF) derived from BCK/AK1 double knock-out animals (BAK −/− MEF) [33]. WT and BAK −/− MEFs at confluence were treated with A-769662, which activated AMPK in less than 30 min as detected by αThr172 phosphorylation (Fig. 5). Immunostaining with anti-P-Ser6 antibody under the very same conditions as for astrocytes revealed a similar central, perinuclear staining in WT MEFs that increased with A-769662 treatment (Fig. 5A,B). The BAK −/− MEFs analyzed under identical conditions did not show any immunofluorescence, neither in control nor in A-769662-treated conditions (Fig. 5C,D). These experiments provide clear evidence for the fluorescence staining corresponding to Ser6-phosphorylated murine BCK.

3.7. P-Ser6 BCK co-localizes with the endoplasmic reticulum

The defined localization of murine BCK in perinuclear regions raised the question whether the Ser-6 phosphorylated BCK species is bound to a specific subcellular structure. Therefore, cellular co-localization of BCK with different marker proteins *in vivo* was studied by confocal microscopy in the primary mouse cortical astrocytes treated with A-769662 or AICAR. Mitochondria and Golgi apparatus are capable to bind small fractions of BCK ([59] and Schlattner et al., unpublished data) and to show perinuclear localization. However, marker proteins for both, mitochondria and Golgi, showed only minimal or incomplete cellular co-localization with phosphorylated BCK (Fig. 6). Only protein disulfide-isomerase (PDI), an ER marker, seemed to fully co-localize with P-Ser6 BCK in confocal 3D-analysis (Fig. 7A–F). Correlation analysis of the two fluorescence channels confirmed strong overlap of both signals (Fig. 7G–K) with very good correlation (Fig. 7M), suggesting that P-Ser6 BCK and PDI indeed co-localize. The 3D data also confirmed the AICAR-induced increase in P-Ser6 BCK which was about 8-fold (Fig. 7L).

Since such confocal analysis is biased by the resolution limits of confocal microscopes, we aimed at additional evidence for close co-localization of P-Ser6 BCK and ER in MEFs. First, we performed classical cellular sub-fractionation of MEFs. In post-mitochondrial fractions enriched for SERCA-containing ER membranes, P-Ser6 BCK was present at low but detectable amounts, and increased upon AICAR treatment (Fig. 8A). Second, we used a proximity ligation assay (PLA) that detects epitopes at a maximal distance of 30–40 nm. When applying antibodies against P-Ser6 BCK and the sarcoplasmic/endoplasmic Ca^{2+}-ATPase SERCA in such PLA experiments, we could detect a significant increase of the fluorescence signal after AICAR-treatment (Fig. 8B–D). Collectively, these data identify the ER as the location of P-Ser6 BCK.

4. Discussion

The brain-type isoform of creatine kinase, BCK, has been identified in this study as a novel AMPK substrate *in vitro* and *in vivo*. Native BCK interacts with active AMPK, leading to BCK phosphorylation at one main site determined to be Ser6. This post-translational modification leaves BCK enzyme activity unaffected, but leads a pool of P-BCK located at ER membranes.

Phosphorylation of CK isoforms, including BCK, has been repeatedly reported in earlier literature [36–38]. More recent proteomics studies suggested specific phosphorylation sites for other CK isoforms, including Ser128 in MCK, possibly targeted by protein kinase C (PKC) [60], Ser319, Ser343, and Thr361 in sMtCK [61], and Tyr115 in uMtCK [62].

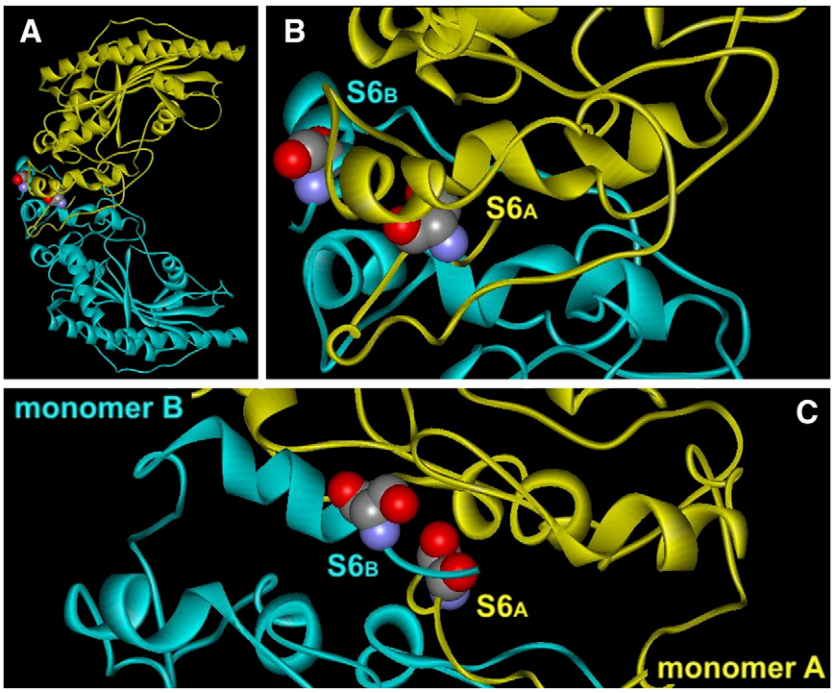

Fig. 9. Localization of the Ser6 phosphosite within the BCK dimeric structure. The high resolution chicken BCK structure [21] is shown in backbone representation with schematic secondary structure elements. (A) Banana-shaped BCK dimer with monomer A in yellow and monomer B in cyan, (B) Close-up of the N-termini at the monomer/monomer interface. Ser6 is represented in CPK representation. Note the divergent N-termini in the two monomers, with monomer B folding inwards thus shielding Ser6 from the surface. (C) Close-up of panel B, rotated by 90° to view the convex side of the dimer. Note: exposure of the hydroxyl function of Ser6 in monomer B. Figure prepared from PDB ID 1QH4 with WebLab ViewerPro 4.0.

However, evidence for the nature of involved protein kinases, phosphorylation stoichiometries, or the resulting functional changes is mostly lacking. In addition, CKs undergo autophosphorylation at multiple residues close to their active site, albeit at very low stoichiometries and without major effects on enzyme catalysis [63,64]. This alone could account for many phosphorylation events as *e.g.* described for MCK in hibernating mammals [65], frog muscle [66] or the diabetic heart [61]. More specifically, PKC was reported to phosphorylate BCK [37,67] and MCK [68,69], but phosphosites were never identified and the physiological relevance remains elusive. Similarly, AMPK was reported to phosphorylate and inhibit MCK, while *vice versa* active MCK by maintaining high PCr/Cr ratios would inhibit AMPK [40]. However, these regulations were not confirmed by follow-up studies [41–43].

In the present study, we present *in vitro* and *in vivo* evidence for BCK phosphorylation by AMPK that involves a different type of regulation. Originating from a non-biased screen [46,47] that already led to confirmed novel AMPK substrates [70], we could identify Ser6 as the BCK phosphosite. This site is conserved across vertebrate species and shows phosphorylation kinetics and stoichiometries that compare favorably with the reference AMPK substrate ACC, suggesting a conserved physiological role of this phosphorylation. Although the Ser6 site does not exactly fit the stringent consensus motif for AMPK [45], it conforms reasonably well to residues identified in a peptide library profiling for an optimal AMPK phosphorylation motif [71]. Comparison of BCK phosphorylation levels with those of ACC suggests one phosphorylation per BCK dimer. This could be very well explained by the molecular structure of BCK that we solved over ten years ago [21]. Although BCK always occurs in homodimeric form, it folds into a structural heterodimer (Fig. 9A). Only one monomer exposes its N-terminus at the convex side of the banana-shaped dimer, while the N-terminus of the second monomer folds back into the monomer/monomer interface (Fig. 9B,C). Thus, effectively only one Ser6 per BCK dimer is accessible for AMPK phosphorylation. Our Y2H interaction data further suggest a sequence of events leading to BCK phosphorylation, in which AMPK is first activated to interact with BCK. As soon as BCK is phosphorylated by bound AMPK, this will trigger its detachment from AMPK, independent of the AMPK phosphorylation state. Since AMPK/BCK interaction can only be detected by Y2H assays and not by co-immunoprecipitation, it is of rather low affinity and rapid 'kiss-and-run' character.

Earlier studies on putative CK phosphorylation tested mainly for enzymatic activity. They reported inhibitions up to 50%, as *e.g.* for PKC- or AMPK-phosphorylated MCK [40,60]. However, ^{31}P NMR spectroscopy of intact rat heart revealed that at increased workload, MCK activity is rather increased than decreased, and positively correlates with higher AMP levels and AMPK activity [41–43]. In the present study, we neither observed any significant change in the catalytic properties of phosphomimetic BCK S6D mutant or BCK in AMPK-activated astrocyte cultures. Generally, it may also be questioned whether minor activity changes reported in earlier studies would be sufficient to effectively regulate this high turnover enzyme *in vivo*. At least heterozygous CK knockout animals with gradually reduced CK levels have no obvious phenotype [72].

Effects of BCK phosphorylation at a subcellular level have not yet been addressed. Only recently, interaction of MCK with the plasma membrane Na^+/Ca^{2+} exchanger has been reported to depend on a putative Ser128 phosphorylation of MCK [69]. In the present study, we analyzed subcellular localization of phospho-BCK in mouse astrocytes and fibroblasts treated with two mechanistically different pharmacological AMPK activators, AICAR or A-769662, and using confocal microscopy, cell fractionation and PLA assays with a specific anti-P-Ser6 BCK antibody. Taken together, the results show that (i) detection of phospho-BCK by anti-P-Ser6 antibody is highly specific as seen with transgenic MEFs lacking BCK, (ii) basic levels of phospho-BCK are low in astrocytes and fibroblasts, (iii) a specific BCK pool is phosphorylated in both cell types after activation of AMPK with the two different activators, and (iv) phospho-BCK localizes to the ER close to the SERCA Ca^{2+}-pump. These data suggest that, during energy stress activating AMPK, a pool of BCK becomes phosphorylated that is localized to the ER. Phosphorylation may trigger recruitment of soluble BCK to the ER, although

one cannot entirely rule out phosphorylation of already ER-located BCK by a highly localized action of AMPK. In either case, BCK phosphorylation could trigger interaction events *via* the change in charge and/or the observed small conformational changes. Ser6 phosphorylation is well located at the convex side of the BCK dimer to engage into interactions without disturbing the active sites located at the opposite, concave side of the dimer (Fig. 9A). The Ser6-site is also close to the domain which in homologous MCK mediates binding to myomesin and M-protein in the myofibrillar M-band [28,29]. Unfortunately, the anti-P-Ser6 antibody is not applicable for co-immunoprecipitation to isolate interaction partners, and future studies will have to identify mechanisms and receptor(s) involved in the BCK/ER interaction.

Specific subcellular localization of BCK has been reported in astrocytes for peripheral regions and pseudopodia, where the enzyme associates with the cytoskeleton and thus contributes to cell shape and motility [33]. BCK also binds to and activates membrane-associated thrombin receptor PAR-1 [35] and a K^+/Cl^- cotransporter [73] at the plasma membrane, and transiently interacts with cis–Golgi matrix protein [59]. At all these specific sites, BCK is expected to locally regenerate ATP for nearby energy-dependent processes. This is particularly important close to membranes, where ATP diffusion may become limiting much earlier during energy stress. We thus propose that BCK phosphorylation is a molecular mechanism to recruit BCK into microcompartments at the ER membrane to sustain ATP-requiring reactions. These may include SERCA that we found co-localized with BCK and for which functional interaction is well established for the highly homologous MCK [74–76]. It can be envisaged that cytosolic Ca^{2+}-overload as occurring under energy-compromised conditions activates the CamKKβ–AMPK signaling cascade to phosphorylate BCK. This could favor interactions bringing BCK in close vicinity of SERCA to support its activity, thus reducing cytosolic Ca^{2+}-overload. ATP consumption by SERCAs may represent up to 20% of whole body total daily energy expenditure [77] and SERCA function strongly depends on a high local ATP/ADP ratio that can be maintained by CK. In support of this model, SERCA activity is reduced in AMPK α2 −/− endothelial cells and can be restored by expressing constitutive active AMPK [78]. However, also other functions of ER-based ATP regeneration are conceivable, as *e.g.* supporting the recently described calcium- and AMPK-controlled ATP-influx into the ER lumen [79].

In conclusion, we have identified a post-translational regulation of BCK by AMPK that involves ER localization. Further investigations are required to determine its importance for ER functions under energy stress *in vivo*.

Acknowledgements

This work was supported by EU FP6 contract LSHM-CT-2004-005272 (EXGENESIS), the French Agence Nationale de Recherche (no. ANR-05-CEXC-014) ('chaire d'excellence' given to US), and CONACYT (Mexico, personal grant no. 183832 to SR). We thank D. Auerbach (Dualsystems Biotech, Schlieren, Switzerland), M. Colombini (Univ. of Maryland, USA), D. G. Hardie (University of Dundee, UK), H. Tokumitsu (Kagawa Medical University, Japan), and B. Wieringa (Nijmegen University, T he Netherlands) for generously providing reagents.

Appendix A. Supplementary data

Supplementary data to this article can be found online at http://dx.doi.org/10.1016/j.bbabio.2014.03.020.

References

[1] D.G. Hardie, F.A. Ross, S.A. Hawley, AMPK: a nutrient and energy sensor that maintains energy homeostasis, Nat. Rev. Mol. Cell Biol. 13 (2012) 251–262.
[2] D. Carling, C. Thornton, A. Woods, M.J. Sanders, AMP-activated protein kinase: new regulation, new roles? Biochem. J. 445 (2012) 11–27.
[3] M.M. Mihaylova, R.J. Shaw, The AMPK signalling pathway coordinates cell growth, autophagy and metabolism, Nat. Cell Biol. 13 (2011) 1016–1023.
[4] J.S. Oakhill, J.W. Scott, B.E. Kemp, AMPK functions as an adenylate charge-regulated protein kinase, Trends Endocrinol. Metab. 23 (2012) 125–132.
[5] D. Carling, F.V. Mayer, M.J. Sanders, S.J. Gamblin, AMP-activated protein kinase: nature's energy sensor, Nat. Chem. Biol. 7 (2011) 512–518.
[6] J.S. Oakhill, R. Steel, Z.P. Chen, J.W. Scott, N. Ling, S. Tam, B.E. Kemp, AMPK is a direct adenylate charge-regulated protein kinase, Science 332 (2011) 1433–1435.
[7] G.J. Gowans, S.A. Hawley, F.A. Ross, D.G. Hardie, AMP is a true physiological regulator of AMP-activated protein kinase by both allosteric activation and enhancing net phosphorylation, Cell Metab. 18 (2013) 556–566.
[8] U. Riek, R. Scholz, P. Konarev, A. Rufer, M. Suter, A. Nazabal, P. Ringler, M. Chami, S.A. Muller, D. Neumann, M. Forstner, M. Hennig, R. Zenobi, A. Engel, D. Svergun, U. Schlattner, T. Wallimann, Structural properties of AMP-activated protein kinase: dimerization, molecular shape, and changes upon ligand binding, J. Biol. Chem. 283 (2008) 18331–18343.
[9] L. Chen, F.J. Xin, J. Wang, J. Hu, Y.Y. Zhang, S. Wan, L.S. Cao, C. Lu, P. Li, S.F. Yan, D. Neumann, U. Schlattner, B. Xia, Z.X. Wang, J.W. Wu, Conserved regulatory elements in AMPK, Nature 498 (2013) E8–E10.
[10] L. Chen, J. Wang, Y.Y. Zhang, S.F. Yan, D. Neumann, U. Schlattner, Z.X. Wang, J.W. Wu, AMP-activated protein kinase undergoes nucleotide-dependent conformational changes, Nat. Struct. Mol. Biol. 19 (2012) 716–718.
[11] G.R. Steinberg, B.E. Kemp, AMPK in health and disease, Physiol. Rev. 89 (2009) 1025–1078.
[12] B. Viollet, S. Horman, J. Leclerc, L. Lantier, M. Foretz, M. Billaud, S. Giri, F. Andreelli, AMPK inhibition in health and disease, Crit. Rev. Biochem. Mol. Biol. 45 (2010) 276–295.
[13] N.B. Ruderman, D. Carling, M. Prentki, J.M. Cacicedo, AMPK, insulin resistance, and the metabolic syndrome, J. Clin. Invest. 123 (2013) 2764–2772.
[14] D.G. Hardie, AMPK: a target for drugs and natural products with effects on both diabetes and cancer, Diabetes 62 (2013) 2164–2172.
[15] U. Schlattner, M. Tokarska-Schlattner, T. Wallimann, Mitochondrial creatine kinase in human health and disease, Biochim. Biophys. Acta 1762 (2006) 164–180.
[16] U. Schlattner, M. Tokarska-Schlattner, S. Ramirez, A. Bruckner, L. Kay, C. Polge, R.F. Epand, R.M. Lee, M.L. Lacombe, R.M. Epand, Mitochondrial kinases and their molecular interaction with cardiolipin, Biochim. Biophys. Acta 1788 (2009) 2032–2047.
[17] T. Wallimann, M. Tokarska-Schlattner, U. Schlattner, The creatine kinase system and pleiotropic effects of creatine, Amino Acids 40 (2011) 1271–1296.
[18] P.P. Dzeja, A. Terzic, Phosphotransfer networks and cellular energetics, J. Exp. Biol. 206 (2003) 2039–2047.
[19] V. Saks, T. Kaambre, R. Guzun, T. Anmann, P. Sikk, U. Schlattner, T. Wallimann, M. Aliev, M. Vendelin, The creatine kinase phosphotransfer network: thermodynamic and kinetic considerations, the impact of the mitochondrial outer membrane and modelling approaches, Subcell. Biochem. 46 (2007) 27–65.
[20] O. Speer, L.J. Neukomm, R.M. Murphy, E. Zanolla, U. Schlattner, H. Henry, R.J. Snow, T. Wallimann, Creatine transporters: a reappraisal, Mol. Cell. Biochem. 256–257 (2004) 407–424.
[21] M. Eder, U. Schlattner, A. Becker, T. Wallimann, W. Kabsch, K. Fritz-Wolf, Crystal structure of brain-type creatine kinase at 1.41 A resolution, Protein Sci. 8 (1999) 2258–2269.
[22] K. Fritz-Wolf, T. Schnyder, T. Wallimann, W. Kabsch, Structure of mitochondrial creatine kinase, Nature 381 (1996) 341–345.
[23] M. Eder, K. Fritz-Wolf, W. Kabsch, T. Wallimann, U. Schlattner, Crystal structure of human ubiquitous mitochondrial creatine kinase, Proteins 39 (2000) 216–225.
[24] J.K. Rao, G. Bujacz, A. Wlodawer, Crystal structure of rabbit muscle creatine kinase, FEBS Lett. 439 (1998) 133–137.
[25] O. Stachowiak, U. Schlattner, M. Dolder, T. Wallimann, Oligomeric state and membrane binding behaviour of creatine kinase isoenzymes: implications for cellular function and mitochondrial structure, Mol. Cell. Biochem. 184 (1998) 141–151.
[26] M. Tokarska-Schlattner, T. Wallimann, U. Schlattner, Multiple interference of anthracyclines with mitochondrial creatine kinases: preferential damage of the cardiac isoenzyme and its implications for drug cardiotoxicity, Mol. Pharmacol. 61 (2002) 516–523.
[27] T. Hornemann, D. Rutishauser, T. Wallimann, Why is creatine kinase a dimer? Evidence for cooperativity between the two subunits, Biochim. Biophys. Acta 1480 (2000) 365–373.
[28] T. Hornemann, S. Kempa, M. Himmel, K. Hayess, D.O. Furst, T. Wallimann, Muscle-type creatine kinase interacts with central domains of the M-band proteins myomesin and M-protein, J. Mol. Biol. 332 (2003) 877–887.
[29] T. Hornemann, M. Stolz, T. Wallimann, Isoenzyme-specific interaction of muscle-type creatine kinase with the sarcomeric M-line is mediated by NH(2)-terminal lysine charge-clamps, J. Cell Biol. 149 (2000) 1225–1234.
[30] F. Streijger, F. Oerlemans, B.A. Ellenbroek, C.R. Jost, B. Wieringa, C.E. Van der Zee, Structural and behavioural consequences of double deficiency for creatine kinases BCK and UbCKmit, Behav. Brain Res. 157 (2005) 219–234.
[31] C.R. Jost, C.E. Van Der Zee, H.J. In 't Zandt, F. Oerlemans, M. Verheij, F. Streijger, J. Fransen, A. Heerschap, A.R. Cools, B. Wieringa, Creatine kinase B-driven energy transfer in the brain is important for habituation and spatial learning behaviour, mossy fibre field size and determination of seizure susceptibility, Eur. J. Neurosci. 15 (2002) 1692–1706.
[32] J.B. Shin, F. Streijger, A. Beynon, T. Peters, L. Gadzala, D. McMillen, C. Bystrom, C.E. Van der Zee, T. Wallimann, P.G. Gillespie, Hair bundles are specialized for ATP delivery via creatine kinase, Neuron 53 (2007) 371–386.
[33] J.W. Kuiper, R. van Horssen, F. Oerlemans, W. Peters, M.M. van Dommelen, M.M. te Lindert, T.L. ten Hagen, E. Janssen, J.A. Fransen, B. Wieringa, Local ATP generation by brain-type creatine kinase (CK-B) facilitates cell motility, PLoS One 4 (2009) e5030.

[34] J.W. Kuiper, H. Pluk, F. Oerlemans, F.N. van Leeuwen, F. de Lange, J. Fransen, B. Wieringa, Creatine kinase-mediated ATP supply fuels actin-based events in phagocytosis, PLoS Biol. 6 (2008) e51.
[35] V.B. Mahajan, K.S. Pai, A. Lau, D.D. Cunningham, Creatine kinase, an ATP-generating enzyme, is required for thrombin receptor signaling to the cytoskeleton, Proc. Natl. Acad. Sci. U. S. A. 97 (2000) 12062–12067.
[36] L.C. Mahadevan, S.A. Whatley, T.K. Leung, L. Lim, The brain isoform of a key ATP-regulating enzyme, creatine kinase, is a phosphoprotein, Biochem. J. 222 (1984) 139–144.
[37] K. Chida, K. Kasahara, M. Tsunenaga, Y. Kohno, S. Yamada, S. Ohmi, T. Kuroki, Purification and identification of creatine phosphokinase B as a substrate of protein kinase C in mouse skin in vivo, Biochem. Biophys. Res. Commun. 173 (1990) 351–357.
[38] A.F. Quest, T. Soldati, W. Hemmer, J.C. Perriard, H.M. Eppenberger, T. Wallimann, Phosphorylation of chicken brain-type creatine kinase affects a physiologically important kinetic parameter and gives rise to protein microheterogeneity in vivo, FEBS Lett. 269 (1990) 457–464.
[39] D. Neumann, U. Schlattner, T. Wallimann, A molecular approach to the concerted action of kinases involved in energy homoeostasis, Biochem. Soc. Trans. 31 (2003) 169–174.
[40] M. Ponticos, Q.L. Lu, J.E. Morgan, D.G. Hardie, T.A. Partridge, D. Carling, Dual regulation of the AMP-activated protein kinase provides a novel mechanism for the control of creatine kinase in skeletal muscle, EMBO J. 17 (1998) 1688–1699.
[41] J.S. Ingwall, Is creatine kinase a target for AMP-activated protein kinase in the heart? J. Mol. Cell. Cardiol. 34 (2002) 1111–1120.
[42] M. Suter, U. Riek, R. Tuerk, U. Schlattner, T. Wallimann, D. Neumann, Dissecting the role of 5′-AMP for allosteric stimulation, activation, and deactivation of AMP-activated protein kinase, J. Biol. Chem. 281 (2006) 32207–32216.
[43] E.B. Taylor, W.J. Ellingson, J.D. Lamb, D.G. Chesser, C.L. Compton, W.W. Winder, Evidence against regulation of AMP-activated protein kinase and LKB1/STRAD/MO25 activity by creatine phosphate, Am. J. Physiol. Endocrinol. Metab. 290 (2006) E661–E669.
[44] U. Riek, S. Ramirez, T. Wallimann, U. Schlattner, A versatile multidimensional protein purification system with full internet remote control based on a standard HPLC system, Biotechniques 46 (2009) ix–xii.
[45] J.W. Scott, D.G. Norman, S.A. Hawley, L. Kontogiannis, D.G. Hardie, Protein kinase substrate recognition studied using the recombinant catalytic domain of AMP-activated protein kinase and a model substrate, J. Mol. Biol. 317 (2002) 309–323.
[46] R.D. Tuerk, R.F. Thali, Y. Auchli, H. Rechsteiner, R.A. Brunisholz, U. Schlattner, T. Wallimann, D. Neumann, New candidate targets of AMP-activated protein kinase in murine brain revealed by a novel multidimensional substrate-screen for protein kinases, J. Proteome Res. 6 (2007) 3266–3277.
[47] R.D. Tuerk, Y. Auchli, R.F. Thali, R. Scholz, T. Wallimann, R.A. Brunisholz, D. Neumann, Tracking and quantification of 32P-labeled phosphopeptides in liquid chromatography matrix-assisted laser desorption/ionization mass spectrometry, Anal. Biochem. 390 (2009) 141–148.
[48] N. Djouder, R.D. Tuerk, M. Suter, P. Salvioni, R.F. Thali, R. Scholz, K. Vaahtomeri, Y. Auchli, H. Rechsteiner, R.A. Brunisholz, B. Viollet, T.P. Makela, T. Wallimann, D. Neumann, W. Krek, PKA phosphorylates and inactivates AMPKalpha to promote efficient lipolysis, EMBO J. 29 (2010) 469–481.
[49] A. Klaus, S. Zorman, A. Berthier, C. Polge, S. Ramirez, S. Michelland, M. Seve, D. Vertommen, M. Rider, N. Lentze, D. Auerbach, U. Schlattner, Glutathione S-transferases interact with AMP-activated protein kinase: evidence for S-glutathionylation and activation in vitro, PLoS One 8 (2013) e62497.
[50] A. Klaus, C. Polge, S. Zorman, Y. Auchli, R. Brunisholz, U. Schlattner, A two-dimensional screen for AMPK substrates identifies tumor suppressor fumarate hydratase as a preferential AMPKalpha2 substrate, J. Proteomics 75 (2012) 3304–3313.
[51] U. Schlattner, M. Eder, M. Dolder, Z.A. Khuchua, A.W. Strauss, T. Wallimann, Divergent enzyme kinetics and structural properties of the two human mitochondrial creatine kinase isoenzymes, Biol. Chem. 381 (2000) 1063–1070.
[52] N. Mockli, A. Deplazes, P.O. Hassa, Z. Zhang, M. Peter, M.O. Hottiger, I. Stagljar, D. Auerbach, Yeast split-ubiquitin-based cytosolic screening system to detect interactions between transcriptionally active proteins, Biotechniques 42 (2007) 725–730.
[53] J. Booher, M. Sensenbrenner, Growth and cultivation of dissociated neurons and glial cells from embryonic chick, and human brain in flask cultures, Neurobiology 2 (1972) 97–105.
[54] U. Schlattner, N. Mockli, O. Speer, S. Werner, T. Wallimann, Creatine kinase and creatine transporter in normal, wounded, and diseased skin, J. Invest. Dermatol. 118 (2002) 416–423.
[55] M. Tokarska-Schlattner, M. Zaugg, R. da Silva, E. Lucchinetti, M.C. Schaub, T. Wallimann, U. Schlattner, Acute toxicity of doxorubicin on isolated perfused heart: response of kinases regulating energy supply, Am. J. Physiol. Heart Circ. Physiol. 289 (2005) H37–H47.
[56] S. Soboll, D. Brdiczka, D. Jahnke, A. Schmidt, U. Schlattner, S. Wendt, M. Wyss, T. Wallimann, Octamer–dimer transitions of mitochondrial creatine kinase in heart disease, J. Mol. Cell. Cardiol. 31 (1999) 857–866.
[57] E.E.M. Manders, F.J. Verbeek, J.A. Aten, Measurement of co-localization of objects in dual-colour confocal images, J. Microsc. 169 (1993) 375–382.
[58] S.P. Davies, A.T. Sim, D.G. Hardie, Location and function of three sites phosphorylated on rat acetyl-CoA carboxylase by the AMP-activated protein kinase, Eur. J. Biochem. 187 (1990) 183–190.
[59] T.S. Burklen, A. Hirschy, T. Wallimann, Brain-type creatine kinase BB-CK interacts with the Golgi matrix protein GM130 in early prophase, Mol. Cell. Biochem. 297 (2007) 53–64.
[60] G. Lin, Y. Liu, K.M. MacLeod, Regulation of muscle creatine kinase by phosphorylation in normal and diabetic hearts, Cell. Mol. Life Sci. 66 (2009) 135–144.
[61] E.S. Boja, D. Phillips, S.A. French, R.A. Harris, R.S. Balaban, Quantitative mitochondrial phosphoproteomics using iTRAQ on an LTQ-Orbitrap with high energy collision dissociation, J. Proteome Res. 8 (2009) 4665–4675.
[62] U. Lewandrowski, A. Sickmann, L. Cesaro, A.M. Brunati, A. Toninello, M. Salvi, Identification of new tyrosine phosphorylated proteins in rat brain mitochondria, FEBS Lett. 582 (2008) 1104–1110.
[63] W. Hemmer, E.M. Furter-Graves, G. Frank, T. Wallimann, R. Furter, Autophosphorylation of creatine kinase: characterization and identification of a specifically phosphorylated peptide, Biochim. Biophys. Acta 1251 (1995) 81–90.
[64] M. Stolz, T. Hornemann, U. Schlattner, T. Wallimann, Mutation of conserved active-site threonine residues in creatine kinase affects autophosphorylation and enzyme kinetics, Biochem. J. 363 (2002) 785–792.
[65] K. Abnous, K.B. Storey, Regulation of skeletal muscle creatine kinase from a hibernating mammal, Arch. Biochem. Biophys. 467 (2007) 10–19.
[66] C.A. Dieni, K.B. Storey, Creatine kinase regulation by reversible phosphorylation in frog muscle, Comp. Biochem. Physiol. B Biochem. Mol. Biol. 152 (2009) 405–412.
[67] K. Chida, M. Tsunenaga, K. Kasahara, Y. Kohno, T. Kuroki, Regulation of creatine phosphokinase B activity by protein kinase C, Biochem. Biophys. Res. Commun. 173 (1990) 346–350.
[68] N. Reiss, J. Hermon, A. Oplatka, Z. Naor, Interaction of purified protein kinase C with key proteins of energy metabolism and cellular motility, Biochem. Mol. Biol. Int. 38 (1996) 711–719.
[69] Y.C. Yang, M.J. Fann, W.H. Chang, L.H. Tai, J.H. Jiang, L.S. Kao, Regulation of sodium–calcium exchanger activity by creatine kinase under energy-compromised conditions, J. Biol. Chem. 285 (2010) 28275–28285.
[70] R. Alzamora, M.M. Al-Bataineh, W. Liu, F. Gong, H. Li, R.F. Thali, Y. Joho-Auchli, R.A. Brunisholz, L.M. Satlin, D. Neumann, K.R. Hallows, N.M. Pastor-Soler, AMP-activated protein kinase regulates the vacuolar H^+-ATPase via direct phosphorylation of the A subunit (ATP6V1A) in the kidney, Am. J. Physiol. Renal Physiol. 305 (2013) F943–F956.
[71] D.M. Gwinn, D.B. Shackelford, D.F. Egan, M.M. Mihaylova, A. Mery, D.S. Vasquez, B.E. Turk, R.J. Shaw, AMPK phosphorylation of raptor mediates a metabolic checkpoint, Mol. Cell 30 (2008) 214–226.
[72] J. van Deursen, W. Ruitenbeek, A. Heerschap, P. Jap, H. ter Laak, B. Wieringa, Creatine kinase (CK) in skeletal muscle energy metabolism: a study of mouse mutants with graded reduction in muscle CK expression, Proc. Natl. Acad. Sci. U. S. A. 91 (1994) 9091–9095.
[73] K. Inoue, S. Ueno, A. Fukuda, Interaction of neuron-specific K^+–Cl^- cotransporter, KCC2, with brain-type creatine kinase, FEBS Lett. 564 (2004) 131–135.
[74] D.O. Levitsky, T.S. Levchenko, V.A. Saks, V.G. Sharov, V.N. Smirnov, The role of creatine phosphokinase in supplying energy for the calcium pump system of heart sarcoplasmic reticulum, Membr. Biochem. 2 (1978) 81–96.
[75] A.M. Rossi, H.M. Eppenberger, P. Volpe, R. Cotrufo, T. Wallimann, Muscle-type MM creatine kinase is specifically bound to sarcoplasmic reticulum and can support Ca^{2+} uptake and regulate local ATP/ADP ratios, J. Biol. Chem. 265 (1990) 5258–5266.
[76] A.J. de Groof, J.A. Fransen, R.J. Errington, P.H. Willems, B. Wieringa, W.J. Koopman, The creatine kinase system is essential for optimal refill of the sarcoplasmic reticulum Ca^{2+} store in skeletal muscle, J. Biol. Chem. 277 (2002) 5275–5284.
[77] S.M. Norris, E. Bombardier, I.C. Smith, C. Vigna, A.R. Tupling, ATP consumption by sarcoplasmic reticulum Ca^{2+} pumps accounts for 50% of resting metabolic rate in mouse fast and slow twitch skeletal muscle, Am. J. Physiol. Cell Physiol. 298 (2010) C521–C529.
[78] Y. Dong, M. Zhang, B. Liang, Z. Xie, Z. Zhao, S. Asfa, H.C. Choi, M.H. Zou, Reduction of AMP-activated protein kinase alpha2 increases endoplasmic reticulum stress and atherosclerosis in vivo, Circulation 121 (2010) 792–803.
[79] N. Vishnu, M. Jadoon Khan, F. Karsten, L.N. Groschner, M. Waldeck-Weiermair, R. Rost, S. Hallstrom, H. Imamura, W.F. Graier, R. Malli, ATP increases within the lumen of the endoplasmic reticulum upon intracellular Ca^{2+} release, Mol. Biol. Cell 25 (2014) 368–379.